Digital Pre- and Post-Equalization for C-Band 112-Gb/s PAM4 Short-Reach Transport Systems

Xizi Tang ¹⁰, Yaojun Qiao ¹⁰, You-Wei Chen ¹⁰, Yueming Lu ¹⁰, and Gee-Kung Chang ¹⁰

Abstract—Insufficient system bandwidth and chromatic dispersion (CD) of fiber are major limitations for high-speed four-level pulse amplitude modulation (PAM4) direct detection systems. In this article, we investigate C-band 112-Gb/s PAM4 optical transport systems over 10-km and 20-km standard single-mode fiber (SSMF) transmission, which suffers from both bandwidth limitation and CD-induced power fading. Advanced digital signal processing techniques are proposed to handle those channel distortions. At the transmitter, a low-complexity $1 + \alpha Z^{-1}$ finite impulse response (FIR) filter coarsely pre-compensates system bandwidth without a preliminary channel estimation. At the receiver, a modified feed-forward equalizer and decision feedback equalizer (FFE-DFE) is employed to compensate residual insufficient bandwidth and CD-induced power fading. Moreover, a novel multi-symbols joint decision is proposed for receiver-side FFE-DFE to mitigate symbol error propagation and correct possible previous error symbols. Experimental results show that the proposed preequalization technique exhibits a better transmission performance, which reduces bit error ratio (BER) from 3.3×10^{-3} to $5.5 \times$ $10^{-4}\ \mathrm{for}$ optical back to back transmission. As for 10-km transmission. sion case, FFE-DFE with 5-symbols joint decision achieves a BER of 7.3×10^{-5} , which is better than the BER of 1.6×10^{-4} with ideal error-propagation-free FFE-DFE (EPF-FFE-DFE). Furthermore, for 20-km transmission scenario, FFE-DFE with 8-symbols joint decision achieves a BER of 6.0×10^{-4} , which is also a superior result than the BER of $9.1 imes 10^{-4}$ with EPF-FFE-DFE.

Index Terms—Error propagation, four-level pulse amplitude modulation (PAM4), pre-equalization, post-equalization.

Manuscript received January 29, 2020; revised March 29, 2020 and April 25, 2020; accepted May 6, 2020. Date of publication May 11, 2020; date of current version September 1, 2020. This work was supported in part by the National Natural Science Foundation of China under Grant 61771062 and Grant 61871044, in part by the Fund of State Key Laboratory of IPOC (BUPT) (IPOC2018ZT08), P. R. China, in part by the BUPT Excellent Ph.D. Students Foundation under Grant CX2019311, and in part by the China Scholarship Council Foundation. (Corresponding author: Yaojun Qiao.)

Xizi Tang is with the State Key Laboratory of Information Photonics and Optical Communications, School of Information and Communication Engineering, Beijing University of Posts and Telecommunications, Beijing 100876, China, and also with the School of Electrical and Computer Engineering, Georgia Institute of Technology, Atlanta, GA 30308 USA (e-mail: tangxizi@bupt.edu.cn).

Yaojun Qiao is with the State Key Laboratory of Information Photonics and Optical Communications, School of Information and Communication Engineering, Beijing University of Posts and Telecommunications, Beijing 100876, China (e-mail: qiao@bupt.edu.cn).

You-Wei Chen and Gee-Kung Chang are with the School of Electrical and Computer Engineering, Georgia Institute of Technology, Atlanta, GA 30308 USA (e-mail: yu-wei.chen@ece.gatech.edu; gkchang@ece.gatech.edu).

Yueming Lu is with the Key Laboratory of Trustworthy Distributed Computing and Service, Ministry of Education, Beijing University of Posts and Telecommunications, Beijing 100876, China (e-mail: ymlu@bupt.edu.cn).

Color versions of one or more of the figures in this article are available online at https://ieeexplore.ieee.org.

Digital Object Identifier 10.1109/JLT.2020.2993997

I. INTRODUCTION

HE fast-emerging services like video streaming, cloud computing and Internet of things are driving the industry to seek a higher capacity solution for the current short-reach optical interconnect scenarios, such as 5G mobile fronthaul, optical access network and data center interconnect [1]. Intensity modulation and direct detection (IM/DD) systems feature small form size, low cost, and low power consumption, which have been widely implemented in the short-reach applications. In order to transmit higher bit rates with limited system bandwidth, advanced modulation formats such as discrete multi-tone (DMT), carrier-less amplitude phase (CAP) modulation and four-level pulse amplitude modulation (PAM4) have been extensively investigated [2]-[4]. Among the aforementioned modulation formats, PAM4 is a promising solution for the upcoming 400-G Ethernet with 8-lane × 50-Gb/s, and the next-generation 800-G Ethernet with 8-lane × 100-Gb/s [5], [6].

In recent years, single-wavelength 50-Gb/s, 100-Gb/s and beyond PAM4 systems have been widely investigated. One of the main challenges for high-speed PAM4 systems is bandwidth limitation. Modified modulation formats, such as Nyquist or faster than Nyquist (FTN) PAM4, and partial-response (PR) PAM4 have been proposed to reduce the effect of bandwidth limitation, since they have lower bandwidth compared to traditional PAM4 signal [7]-[9]. Besides, electrical equalizations based on digital signal processing (DSP) techniques are effective ways to eliminate inter-symbol interference (ISI) caused by bandwidth limitation. The electrical equalizations could be deployed either in transmitter side or receiver side. However, electrical pre-equalization generally requires an accurate channel estimation [10], [11]. On the other hand, another main distortion for PAM4 systems is severe power fading caused by chromatic dispersion (CD) of fiber and square-law detection of photo-detector [12]. Although systems operated at O-band could avoid severe CD distortion, C-band transmission has the advantages of lower fiber loss, mature wavelength division multiplexing (WDM) optics and optical amplifiers [13], [14]. Therefore, extensive modification works such as optical dispersion compensation fiber (DCF), Kramers-Kronig receiver, CD pre-compensation, and single sideband or vestigial sideband (SSB/VSB) modulation have been implemented to cope with the effect of CD [15]. However, these methods require complex system architecture and additional expensive devices, which are not cost-effective solutions for short-reach optical interconnect systems.

0733-8724 © 2020 IEEE. Personal use is permitted, but republication/redistribution requires IEEE permission. See https://www.ieee.org/publications/rights/index.html for more information.

TABLE I
RECENT TRANSMISSION RESULTS FOR C-BAND 56-Gb/s AND 112-Gb/s PAM4
SYSTEMS WITH ONLY ADVANCED DSP TECHNIQUES

Reference	Bitrate (Gb/s)	DSP techniques	Distance (km)
[16]	56	Pre-compensation & MLSE	26.4
[17]	56	LDPC Code & Soft-output MLSE	30
[18]	56	pre-FFE & ID-FFE/ID-DFE	43
[19]	56	THP & FFE/Volterra	80
[20]	56	MPE-DFE	80
[21]	112	DB-PAM4 & TS-LMS	1
[22]	112	CS-PAM4 & Volterra	5
[23]	112	Transmitter-side Volterra	8
This work	112	2-tap Pre-equalization & Modified FFE-DFE	10 & 20

Applying advanced DSP techniques could improve CD tolerance and extend transmission distance for IM/DD systems, which is a potential low-cost solution for handing CD distortion because it is closely compatible to the traditional architecture of IM/DD systems. Table 1 shows some of recent experimental results for C-band 56-Gb/s and 112-Gb/s PAM4 systems with only advanced DSP techniques to improve CD tolerance [16]–[23]. For 56-Gb/s PAM4 systems, Ref. [16] and [17] demonstrated transmission results with hard-output MLSE and soft-output MLSE, respectively. However, both transmission distances are limited to 30 km. Ref. [18] proposed an intensity directed equalizer based on FFE and decision feedback equalizer (ID-FFE/ID-DFE), which enabled 56-Gb/s PAM4 up to 43-km transmission. Ref. [19] employed Tomlinson-Harashima precoding (THP) at transmitter to resist CD-induced power fading, which achieved 56-Gb/s PAM4 over 80-km standard single-mode fiber (SSMF) transmission. Similarly, our previous work also demonstrated 56-Gb/s PAM4 over 80-km SSMF transmission with modified memory polynomial equalizer (MPE) combined with decision feedback equalizer (MPE-DFE) [20]. However, when the bitrate further increases to 112 Gb/s, the effect of CD is much more severe. Ref. [21] demonstrated a C-band 112-Gb/s duo-binary PAM4 (DB-PAM4) signal over 1-km SSMF transmission with directly modulated laser (DML) and training sequence aided least-mean square (TS-LMS) algorithm. Ref. [22] reported a result of C-band 112-Gb/s constellation switching PAM4 (CS-PAM4) over 5-km transmission with Volterra equalizer. Ref. [23] employed a transmitter side Volterra equalizer, which can support a C-band 112-Gb/s PAM4 over approximate 8-km SSMF transmission. These results reveal that transmission distances for C-band 112-Gb/s PAM4 systems are generally limited to below 10 km.

Our previous work demonstrated a C-band 112-Gb/s PAM4 over 20-km SSMF transmission with coefficient-updated FFE-DFE with erasure technology [24]. In this paper, we modified and extended this work using coefficient-stable FFE-DFE with multi-symbols joint decision technique. The

experimental results of both 10-km and 20-km SSMF transmission are presented. Moreover, improved transmission performance is achieved compared with the previous work. The main contributions and impacts of this paper can be summarized as follows:

- At transmitter, we propose to use a low-complexity 2tap finite impulse response (FIR) filter to coarsely precompensate bandwidth limitation, which doesn't rely on a preliminary channel estimation.
- At receiver, post-equalization based on modified FFE-DFE is proposed to flexibly compensate residual insufficient bandwidth and CD-induced deep spectrum nulls.
- A novel multi-symbols joint decision is proposed for receiver-side FFE-DFE, which could mitigate symbol error propagation and correct previous error symbols.
- Experimental results show that the proposed preequalization greatly optimizes transmission performance, which reduces bit error ratio (BER) from 3.3×10^{-3} to 5.5×10^{-4} for optical back to back (OBTB) transmission.
- For 10-km SSMF transmission, the receiver-side FFE-DFE with 5-symbols joint decision achieves a BER of 7.3×10^{-5} , which is lower than that of 1.6×10^{-4} with ideal error-propagation-free FFE-DFE (EPF-FFE-DFE).
- For 20-km SSMF transmission, the receiver-side FFE-DFE with 8-symbols joint decision achieves a superior BER of 6.0×10^{-4} compared with the BER of 9.1×10^{-4} with EPF-FFE-DFE.

The rest of this paper proceeds as follows. The principle of CD-induced power fading is analyzed in Section II. In Section III, the experimental setup and principle of DSP are presented. In Section IV, we analyze and discuss the experimental results with digital equalization techniques for OBTB transmission, 10-km SSMF transmission and 20-km SSMF transmission, respectively. Finally, the paper is concluded in Section V.

II. PRINCIPLE OF CD-INDUCED POWER FADING

Generally, a double-side band (DSB) optical signal S(w) in frequency domain can be expressed as [25]:

$$S(w) = e^{jw_0t}(ae^{jwt} + a^*e^{-jwt} + C)$$
 (1)

in which a represents the data at baseband frequency w, C is the direct-current (DC) bias, and w_0 is the optical carrier. It is well-known that transfer function of fiber can be written as:

$$H(\omega) = exp\left(-j\frac{\lambda^2}{4\pi c}DL\omega^2\right) = exp\left(-j\frac{\beta_2}{2}L\omega^2\right)$$
 (2)

where λ is the optical carrier wavelength, c is the velocity of light, D is the dispersion coefficient, L is the fiber length, and β_2 is the group velocity parameter. Therefore, the optical signal after fiber transmission can be expressed as

$$X(w) = e^{jw_0 t} \left(a e^{jwt} e^{\left(-j\frac{\beta_2}{2}L\omega^2 \right)} + a^* e^{-jwt} e^{\left(-j\frac{\beta_2}{2}L\omega^2 \right)} + C \right)$$

Since the square-law detection is applied to achieve photovoltaic conversion, the received electrical signal can be expressed as

$$Y(w) = X(w)X^*(w) \tag{4}$$

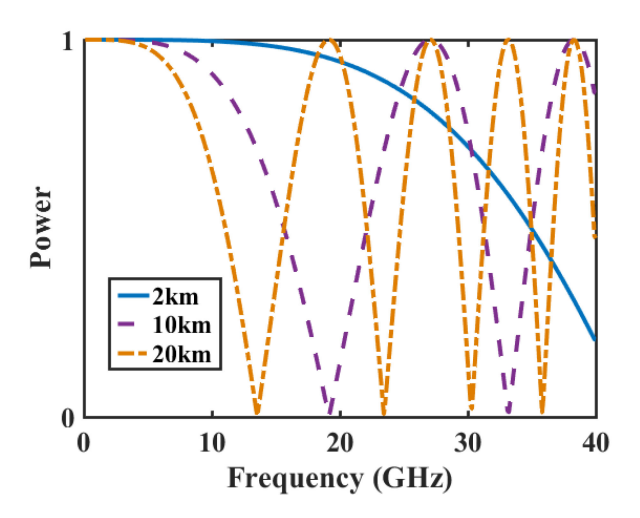


Fig. 1. The frequency response of CD-induced power fading for different fiber lengths.

By substituting Eq. (3) for X(w) in Eq. (4), we can obtain many terms. For simplicity, the DC terms and signal to signal beating terms are ignored. Here, we only consider the desired first-order terms of signal and Y(w) is calculated as

$$Y(w) = 2aC\cos\left(\frac{\beta_2}{2}L\omega^2\right)\left(e^{jwt} + e^{-jwt}\right) \tag{5}$$

Finally, the normalized power fading of fiber in frequency domain can be expressed as

$$H(f) = \cos(2\pi^2 \beta_2 L f^2) \tag{6}$$

where $\beta_2=-2.16\times 10^{-26}s^2/m$ for the optical wavelength of 1550 nm, L is fiber length and f is signal frequency.

In order to visualize the effect of CD-induced power fading, Fig. 1 shows the normalized frequency response of CD for different fiber lengths. Typical short-reach optical interconnect transmission distances of 2-km, 10-km and 20-km are considered. It can be found that for 2-km transmission, the first spectrum null is beyond 40 GHz. However, the first spectrum nulls for 10-km and 20-km transmission are 19.2 GHz and 13.6 GHz, respectively. Note that they are located within the Nyquist frequency of 28 GHz, which undoubtedly would cause severe distortion for 112-Gb/s PAM4 signal.

III. EXPERIMENTAL SETUP AND DSP

A. Experimental Setup

Fig. 2 shows the experimental setup of C-band 112-Gb/s PAM4 IM/DD system. At transmitter, the offline generated PAM4 data was loaded to a 100-GSa/s arbitrary waveform generator (AWG) with 35-GHz bandwidth. After that, the generated electrical signal was amplified by a fixed gain of 19-dB driver with 25-GHz bandwidth. Then, we used a 6-dB electrical attenuator to appropriately reduce signal amplitude. A laser with a central wavelength of 1550.12 nm was employed to generate the optical carrier. A Mach-Zehnder modulator (MZM) was used to modulate the electrical signal into the optical domain. The V_{π} of MZM is approximately 3.5 V and the DC bias was set to make the modulation signal at the linear region. The output

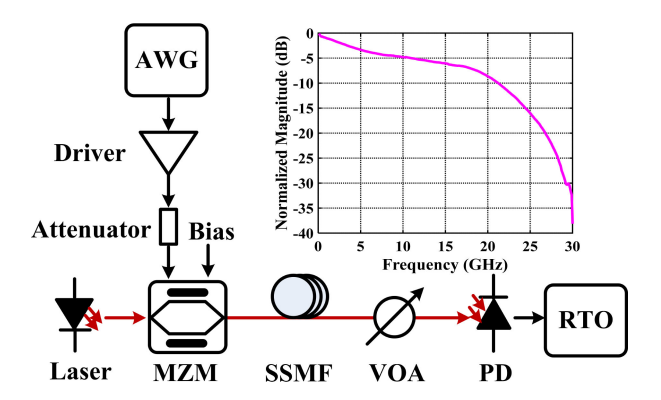


Fig. 2. Experimental setup of C-band 112-Gb/s PAM4 intensity modulation and direct detection (IM/DD) system. AWG: Arbitrary waveform generator; MZM: Mach-Zehnder modulator; SSMF: Standard single-mode fiber; VOA: Variable optical attenuator; PD: Photo-detector; RTO: Real-time oscilloscope.

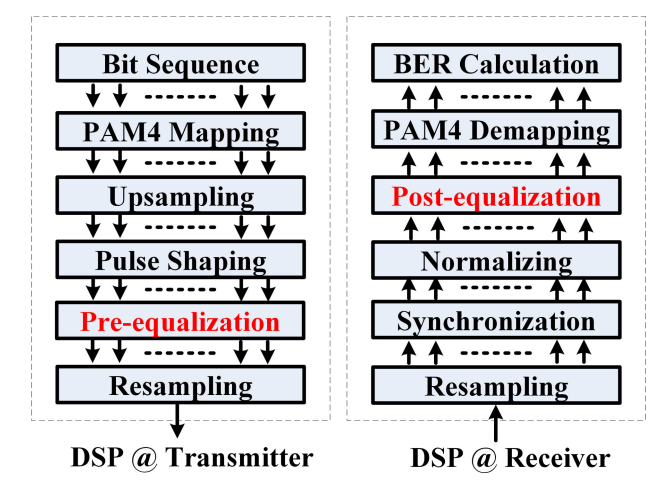
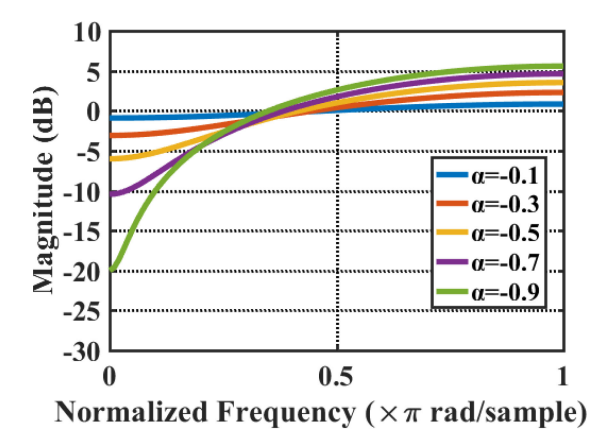


Fig. 3. DSP flow at transmitter and receiver with MATLAB.

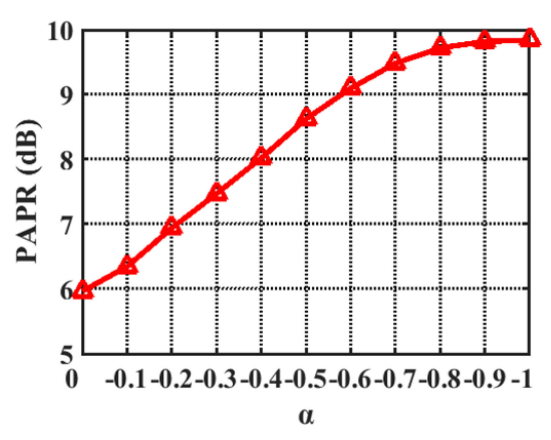
optical power of MZM was around +4 dBm. Afterwards, the optical signal was launched into SSMF for transmission. At receiver, a variable optical attenuator (VOA) was applied to adjust received optical power and a photo-detector (PD) with 20-GHz bandwidth was employed to achieve photoelectric conversion. Then, the electrical signal is captured by a 63-GHz real-time oscilloscope (RTO) with 8-bits resolution and 160-GSa/s sampling rate. Finally, the offline DSP was finished with MATLAB, which mainly includes resampling, synchronization, normalizing, post-equalization, PAM4 demapping, and BER calculation. The system frequency response at OBTB transmission is also shown in the inset of Fig. 2. It can be found that the whole system is of around -3 dB bandwidth of 5 GHz and -10 dB bandwidth of 21 GHz.

B. Pre-equalization at Transmitter

Fig. 3 shows the DSP flow at transmitter and receiver. At the transmitter side, every 72400 bits are mapped to one PAM4 frame with Gray code. Note that the first 1000 PAM4 symbols are considered as training sequence for the receiver-side equalization. Afterwards, the PAM4 signal is up-sampled with a factor of 2. Then, a square root-raise-cosine (RRC) filter with a factor of 0.4 is applied to do Nyquist pulse shaping in the time domain. In the next step, a 2-tap FIR pre-filter is employed to



(a) Frequency response of pre-filter with different $\boldsymbol{\alpha}$ value



(b) Signal PAPR after pre-filter with different α value

Fig. 4. (a). Frequency response of pre-filter with different α value; (b). Signal PAPR after pre-filter with different α value.

do channel pre-equalization. The Z-domain expression of 2-tap FIR pre-filter can be written as

$$H_{pre-filter} = 1 + \alpha Z^{-1} \tag{7}$$

The normalized frequency response of pre-equalization with different α value is depicted in Fig. 4(a). It can be found that the pre-filter would enhance high-frequency response while decrease low-frequency response. The frequency response varies according to the α value. In addition to the change of frequency response, however, pre-equalization would also cause a growth in signal peak to average power ratio (PAPR), which can be seen in Fig. 4(b). When α value goes from 0 to -1, the PAPR increases from 6 dB to approximately 10 dB.

The adopted 2-tap FIR pre-filter has the following two advantages compared to pre-equalization with the inverse of channel response: 1) The 2-tap FIR pre-filter doesn't require accurate channel estimation and channel feedback. 2) The computational complexity of pre-equalization is extremely low since only a 2-tap FIR filter is applied.

C. Post-equalization at Receiver

In this paper, a modified FFE-DFE is proposed for mitigating residual bandwidth limitation and CD-induced power fading at

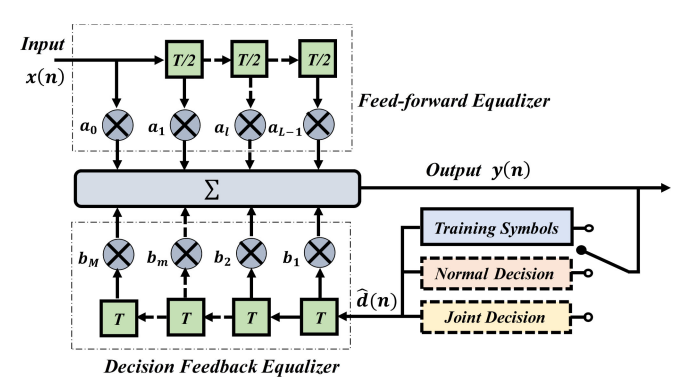


Fig. 5. Illustrative structure of modified FFE-DFE.

receiver. Note that T/2 symbol space is applied to FFE to provide robustness against clock jitter while T symbol space is used to DFE. The illustrative structure of FFE-DFE can be seen in Fig. 5 and mathematical expression of FFE-DFE can be written as

$$y(n) = \sum_{l=0}^{L-1} a_l \times x(2n-l) + \sum_{m=1}^{M} b_m \times \widehat{d}(n-m)$$

$$Feed-forward\ terms$$
(8)

in which x(n) is the T/2 input signal, $\widehat{d}(n)$ denotes the decision feedback signal, y(n) represents the output signal, and a_l and b_m are tap coefficients of feed-forward terms and decision-feedback terms, respectively. L and M are feed-forward and decision-feedback tap numbers, respectively. Hence, the FFE-DFE with different taps could be noted as FFE-DFE(L,M). It is well-known that FFE-DFE generally achieves better performance than single FFE owing to feedback structure to mitigate enhanced noise [26]. Moreover, DFE could be viewed as an autoregressive (AR) filter which compensates spectrum nulls by inserting poles [27].

However, one major problem of FFE-DFE is error propagation when wrong decision symbols are fed to DFE. It is universally acknowledged that when output symbols are far from the constellation points, it is more likely to get wrong decision symbols. Therefore, we could define an unreliable region according to the distance between the output symbols and constellation points. The minimum distance can be calculated as

$$\varepsilon_r = min|y(n) - SigConst| \tag{9}$$

where y(n) is output symbol and SigConst is possible decision symbols (+3,+1,-1,-3) for PAM4 symbols. Here, a specific value is defined as the distance threshold D_T . If the minimum distance ε_r is smaller than the distance threshold D_T , we consider the symbol as a reliable decision symbol. Otherwise, if ε_r is greater than the distance threshold D_T , we consider the symbol as an unreliable decision symbol.

The proposed modified FFE-DFE can be operated in one of three modes, which can be seen in the bottom right of Fig. 5. Firstly, we use recursive least square (RLS) adaptive algorithm and training symbols to update tap coefficients for equalizer convergence. This is called training symbols mode. In this stage,

known training symbols are fed to DFE to achieve no error propagation. When the equalizer has been successfully converged, training symbols are not required anymore. Afterwards, the equalizer could be categorized into two types: coefficient-updated equalizer or coefficient-stable equalizer. The difference is the former would continuously update equalizer coefficients according to mean square errors (MSE) while the latter would not. It is noted that we adopt coefficient-stable equalizer in this work.

Then, the operation mode of equalizer is dependent on whether the output symbol is located in reliable region. If the output symbol is located in reliable region, the decision is operated in a normal decision mode and the equalizer is exactly the traditional FFE-DFE. However, if the output symbol falls in the unreliable region, the equalizer is operated in a joint decision mode. At this time, multi-symbols joint decision is applied to further determine the output symbol and decision symbol. Let us assume that we enter joint decision mode for output symbol y(n) and we want to consider (N+1)-symbols joint decision. In order to obtain (N + 1) output symbols for joint decision, we feed the decision symbols '0' to the DFE to obtain the next Noutput symbols; i.e., we set $\widehat{d}(n+i) = 0, i = 0, \dots, N-1$ till we collect (N+1) output symbols $y(n), \ldots, y(n+N)$. Here, we take 3-symbols joint decision as an example. The error value is defined as the difference between output symbol and decision symbol, which can be calculated as

$$e(n) = y(n) - \widehat{d}'(n) \tag{10}$$

$$e(n+1) = y(n+1) + b_1 \hat{d}'(n) - \hat{d}'(n+1)$$
(11)

$$e(n+2) = y(n+2) + b_2 \hat{d}'(n) + b_1 \hat{d}'(n+1) - \hat{d}'(n+2)$$
(12)

we could rewrite Eq. (10)-Eq. (12) and extend to N+1 symbols joint decision in matrix form:

$$\begin{bmatrix} e(n) \\ e(n+1) \\ e(n+2) \\ \dots \\ e(n+N) \end{bmatrix} = \begin{bmatrix} y(n) \\ y(n+1) \\ y(n+2) \\ \dots \\ y(n+N) \end{bmatrix} - \begin{bmatrix} 1 & 0 & \cdots & 0 \\ -b_1 & 1 & \cdots & 0 \\ -b_2 & -b_1 & \cdots & 0 \\ \vdots & \vdots & \ddots & \vdots \\ -b_N & -b_{N-1} & \cdots & 1 \end{bmatrix} \begin{bmatrix} \widehat{d'}(n) \\ \widehat{d'}(n+1) \\ \widehat{d'}(n+2) \\ \vdots \\ \widehat{d'}(n+N) \end{bmatrix}$$
(13)

where $\widehat{d'}(n+i), i=0,\dots,N$ denote the candidate decision symbols. The optimal solution of Eq. (13) can be obtained based on the maximum likelihood (ML) principle to achieve minimum MSE, i.e., $\frac{1}{N+1}\sum_{i=0}^N e(n+i)^2$. After that, the previous unreliable output symbols and previous decision symbols are corrected by the joint decision symbols. In this way, we could obtain more reliable decision symbols, thus mitigating possible error propagation and correct possible previous error symbols.

In terms of complexity, since multiplication complexity is much higher than addition complexity, the number of multiplications and comparisons are mainly evaluated. For (N+1)-

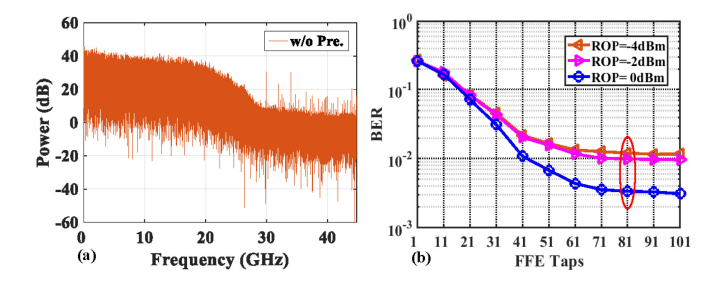


Fig. 6. (a). Received signal frequency spectrum for OBTB transmission without pre-equalization; (b). BER versus FFE taps for OBTB transmission without pre-equalization.

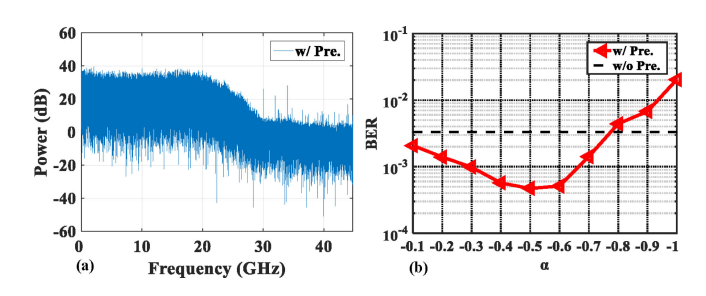


Fig. 7. (a). Received signal frequency spectrum for OBTB transmission with pre-equalization of $1-0.5Z^{-1}$; (b). BER versus different α for pre-equalization at received optical power of 0 dBm.

symbols joint decision, firstly, we need (L+M)(N+1) multiplications to obtain previous output symbols y. Then, 2N(N+1) multiplications are needed to calculate errors from e(n) to e(n+N). Afterwards, $4(4^{N+1}-1)/3$ multiplications are required to get the square errors. Finally, we need $4^{N+1}-1$ comparisons to choose the path has minimum MSE. Therefore, we need $(L+M)(N+1)+2N(N+1)+4(4^{N+1}-1)/3$ multiplications and $4^{N+1}-1$ comparisons for each joint decision output symbol, which reveals that the complexity grows exponentially by N.

IV. EXPERIMENTAL RESULTS AND DISCUSSIONS

A. Experimental results for OBTB Transmission

Fig. 6(a) shows the received signal frequency spectrum without pre-equalization. It can be found that the received signal suffers from high-frequency distortion since the experimental system is bandwidth-limited. In order to compensate for the insufficient bandwidth, FFE with different taps are investigated to equalize high-frequency distortion. Fig. 6(b) shows BER performance versus different tap numbers at received optical power of -4/-2/0 dBm, respectively. It depicts that 81 taps could be chosen as optimal tap numbers considering a tradeoff between equalization performance and computational complexity. However, as it is known to all, FFE would increase high-frequency noise as well when the insufficient system bandwidth is compensated. Therefore, the achieved BER with FFE is limited to 3.3×10^{-3} .

Fig. 7(a) shows the received signal frequency spectrum with the proposed 2-tap FIR pre-filter. It reveals that the signal

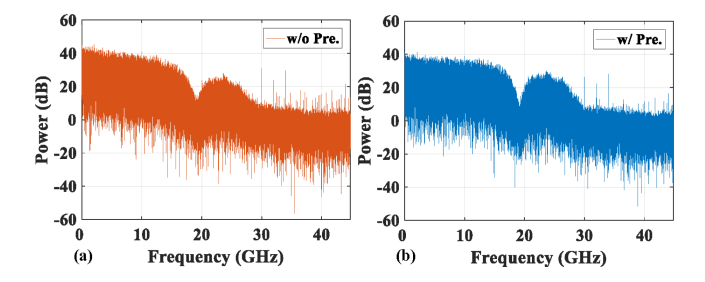


Fig. 8. (a). Received signal frequency spectrum for 10-km SSMF transmission without pre-equalization; (b). Received signal frequency spectrum for 10-km SSMF transmission with pre-equalization.

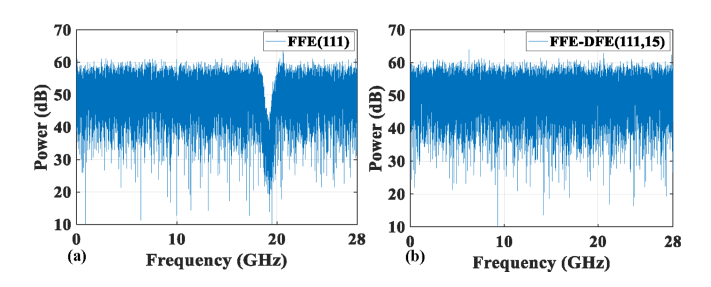


Fig. 9. (a). Recovered signal frequency spectrum with FFE(111); (b). Recovered signal frequency spectrum with FFE-DFE(111,15).

frequency spectrum is flatter than that without pre-equalization in Fig. 6(a). Since the proposed 2-tap FIR pre-filter is not an accurate channel compensation, FFE is still required to compensate residual bandwidth limitation. However, the noise enhancement would be alleviated by bandwidth pre-compensation. Fig. 7(b) shows the BER performance versus different α for pre-equalization at received optical power of 0 dBm. Note that FFE with 81 taps is still used to compensate residual bandwidth limitation. It depicts that pre-equalization with α ranging from -0.1 to -0.7 achieves better BER performance compared to that without pre-equalization. The optimal BER performance is achieved at the α of -0.5 with the BER of 5.5×10^{-4} . Thanks to an OBTB performance sweeping over the different α values, the proposed pre-equalization enables optimized transmission performance and is applied to the following experimental system unless otherwise explicitly indicated.

B. Experimental results for 10-km SSMF transmission

Fig. 8(a) and Fig. 8(b) show the received signal frequency spectrum after 10-km SSMF transmission without and with pre-equalization respectively. Due to the effect of CD-induced power fading, the signal frequency spectrum suffers from deep spectrum nulls, where the first spectrum null is located in around 19.2 GHz, no matter with or without pre-equalization. Therefore, although the pre-equalization is able to partly compensate limited bandwidth, it cannot equalize CD-induced spectrum null.

Fig. 9 shows the recovered frequency spectrum with FFE(111) and FFE-DFE(111,15) at the received optical power of 0 dBm, respectively. FFE(111) represents FFE with 111 taps while FFE-DFE(111,15) denotes FFE-DFE with 111 feed-forward taps and 15 feedback taps. It is noted that the tap numbers have

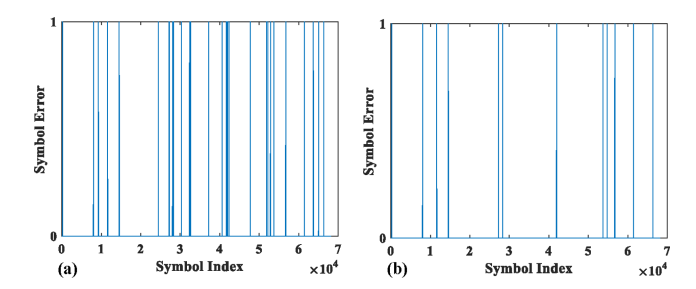


Fig. 10. (a). Symbol errors for FFE-DFE(111,15); (b). Symbol errors for EPF-FFE-DFE(111,15).

been optimized considering equalization performance and computational complexity. Fig. 9(a) depicts that the spectrum null still exists since linear FFE cannot equalize deep spectrum null. Fortunately, FFE-DFE can fundamentally compensate spectrum null owing to its function of inserting pole [27]. Hence, it can be seen in Fig. 9(b) that signal spectrum null is successfully compensated with FFE-DFE(111,15).

As we mentioned, FFE-DFE may have the problem of error propagation owing to incorrect symbol feedback to DFE. Fig. 10(a) and Fig. 10(b) show the output error symbols for FFE-DFE(111,15) and error-propagation-free (EPF) FFE-DFE(111,15), respectively. The EPF-FFE-DFE is defined as FFE-DFE without error propagation, which adopts all of the transmitter data as training symbols in order to make sure all the feedback symbols are correct. It could be found that there are some successive symbol errors in Fig. 10(a) while symbol errors in Fig. 10(b) are fewer and more independent. The reason could be attributed to that incorrect decision symbols with traditional FFE-DFE(111,15) give rise to error propagation while EPF-FFE-DFE(111,15) doesn't have this problem. However, it's essential to note that it is impossible to use all of the sending data as training symbols to achieve EPF-FFE-DFE in practical application. In order to measure the degree of error propagation, average error propagation length L_{EP} could be defined as [27]

$$L_{EP} = \frac{SER_{EP}}{SER_{EPF}} - 1 \tag{14}$$

in which SER_{EP} represents symbol error ratio (SER) with FFE-DFE and SER_{EPF} denotes SER with EPF-FFE-DFE.

Fig. 11(a) shows the relationship between error propagation length L_{EP} and distance threshold D_T when applying FFE-DFE with different symbols joint decision. The distance threshold D_T is used to measure the size of unreliable region. When the distance threshold D_T is equal to 0, all of the output symbols are located in unreliable region and the equalizer only operates in joint decision mode. However, when the distance threshold D_T is equal to 1, the equalizer almost always operates in the normal decision mode. Fig. 11(a) also depicts that when distance threshold D_T is less than 0.8, the average error propagation lengths are almost the same. Besides, when more symbols are applied to joint decision, the average error propagation length can be significantly decreased. This could be attributed to that more symbols joint detection leads to less likely incorrect decision and less error propagation. It is interesting to observe that when 5-symbols joint decision is used, average error propagation

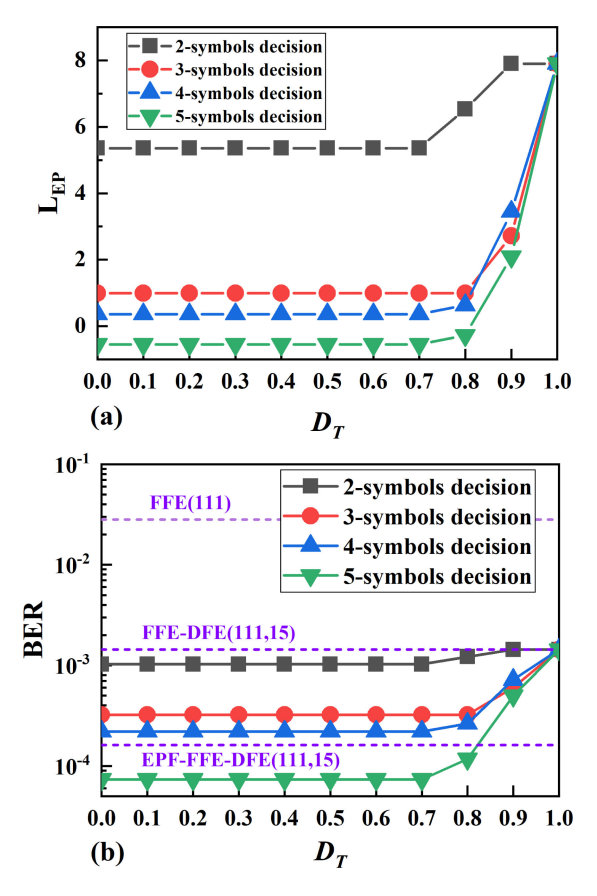


Fig. 11. (a). Error propagation length versus distance threshold with different symbols joint detection for 10-km SSMF transmission; (b). BER versus distance threshold with different symbols joint detection for 10-km SSMF transmission.

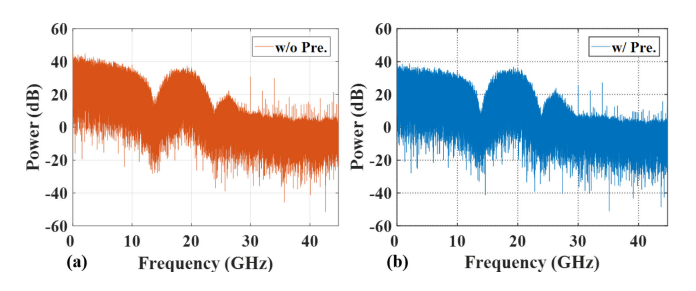


Fig. 12. (a). Received signal frequency spectrum for 20-km SSMF transmission without pre-equalization; (b). Received signal frequency spectrum for 20-km SSMF transmission with pre-equalization.

length $L_{EP} < 0$ can be achieved, which means which means the SER of FFE-DFE with 5-symbols joint decision is less than that of EPF-FFE-DFE. This is because the joint symbol decision not only mitigates error propagation, but also corrects previous error symbols. In other words, although EPF-FFE-DFE will not lead to error propagation, it cannot correct the existed error symbols, either. However, joint symbols decision has the ability to correct the previous error symbols.

Fig. 11(b) shows the BER versus distance threshold D_T when applying FFE-DFE with different symbols joint decision. Moreover, the achieved BERs with traditional FFE(111), FFE-DFE(111,15) and EPF-FFE-DFE(111,15) are 2.8×10^{-2} , 1.4×10^{-3} and 1.6×10^{-4} respectively, which have been plotted in Fig. 11(b) to give an explicit comparison with FFE-DFE with joint decision. The BER with joint decision in Fig. 11(b)

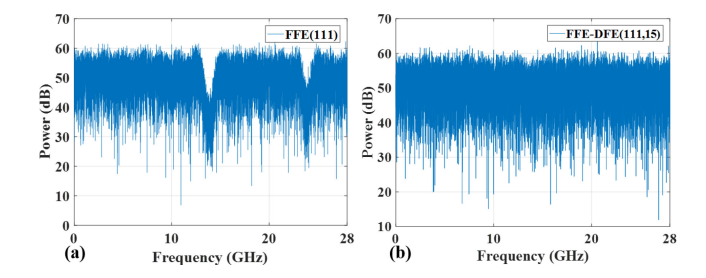


Fig. 13. (a). Recovered signal frequency spectrum with FFE(111); (b). Recovered signal frequency spectrum with FFE-DFE(111,15).

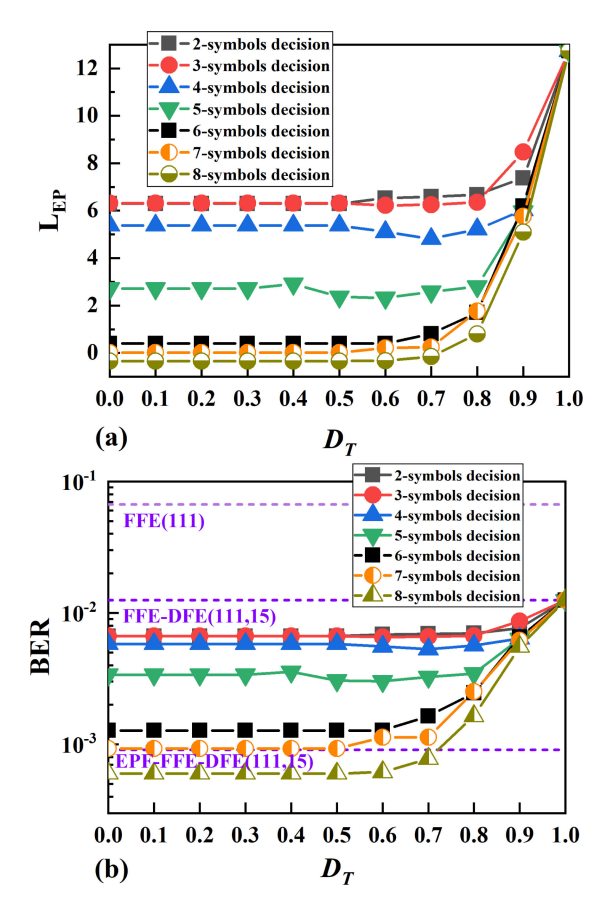


Fig. 14. (a). Error propagation length versus distance threshold with different symbols joint detection for 20-km SSMF transmission; (b). BER versus distance threshold with different symbols joint detection for 20-km SSMF transmission.

shows a strong consistency with L_{EP} in Fig. 11(a). Similarly, 5-symbols joint decision shows a better BER of 7.3×10^{-5} than the BER of 1.6×10^{-4} with ideal EPF-FFE-DFE(111,15), since joint decision could correct previous error symbols.

C. Experimental Results for 20-km SSMF Transmission

Fig. 12(a) and Fig. 12(b) show the signal frequency spectrum after 20-km SSMF transmission without and with preequalization respectively. Different from 10-km SSMF transmission, signal frequency spectrum after 20-km SSMF transmission has two spectrum nulls within its Nyquist bandwidth, which means signal suffers from more CD distortion. Moreover, pre-equalization cannot compensate spectrum nulls either. Fig. 13 shows the recovered frequency spectrum with FFE(111) and FFE-DFE(111,15) at received optical power of 0 dBm, respectively. Fig. 13(a) depicts the two spectrum nulls cannot be compensated by FFE(111) while Fig. 13(b) shows FFE-DFE(111,15) can compensate both of two spectrum nulls.

Similarly, Fig. 14(a) shows the average error propagation length L_{EP} versus distance threshold D_T using FFE-DFE with different symbols joint decision for 20-km SSMF transmission. Traditional FFE-DFE without joint decision $(D_T \ge 1)$ has an average error propagation length of 12.7, while 8-symbols joint decision could reduce the L_{EP} to below 0 when the distance threshold D_T is less than 0.8. Fig. 14(b) shows the relationship between BER and distance threshold D_T when applying FFE-DFE with different symbols joint decision. The achieved BERs with FFE(111), FFE-DFE(111,15) and EPF-FFE-DFE(111,15) of 6.7×10^{-2} , 1.2×10^{-2} and 9.1×10^{-4} are plotted for comparison, respectively. It can be found that FFE-DFE with 8symbols joint decision achieve a superior BER of 6.0×10^{-4} than that of 9.1×10^{-4} with EPF-FFE-DFE. It is noted that up to 8-symbols joint decision suffers from huge complexity to achieve improved performance than EPF-FFE-DFE. In practical application, trade-off between complexity and performance should be considered. Otherwise, further research is required to reduce complexity of the equalizer.

V. CONCLUSION

In this work, we have successfully demonstrated C-band 112-Gb/s PAM4 signal over 10-km and 20-km SSMF transmission with digital pre- and post-equalization. A simple 2tap $(1-0.5Z^{-1})$ FIR filter is employed at the transmitter to pre-compensate insufficient system bandwidth. At the receiver, modified FFE-DFE is applied to compensate residual bandwidth limitation and CD-induced power fading. Moreover, a novel multi-symbols joint decision is proposed for FFE-DFE to mitigate error propagation and correct previous error symbols. Experimental results show that 5-symbols joint decision FFE-DFE achieves a BER of 7.3×10^{-5} for 10-km transmission while FFE-DFE with 8-symbols joint decision achieves a BER of 6.0×10^{-4} for 20-km transmission. Both measured BERs are below 7% feed-forward error correction threshold of 3.8×10^{-3} and also superior to the BERs with EPF-FFE-DFE. We believe that the proposed equalization techniques show great potential in the high-speed, short-reach PAM4 optical transport systems.

ACKNOWLEDGMENT

The authors would like to thank the support of laboratory equipment provided by Prof. Fan Zhang in Peking University.

REFERENCES

- G. Liu, L. Zhang, T. Zuo, and Q. Zhang, "IM/DD transmission techniques for emerging 5G fronthaul, DCI, and metro applications," *J. Lightw. Technol.*, vol. 36, no. 2, pp. 560–567, 2018.
- [2] K. Zhong et al., "Experimental study of PAM-4, CAP-16, and DMT for 100Gb/s short reach optical transmission systems," Opt. Express, vol. 23, no. 2, pp. 1176–1189, 2015.
- [3] J. Shi, J. Zhang, Y. Zhou, Y. Wang, N. Chi, and J. Yu, "Transmission performance comparison for 100-Gb/s PAM-4, CAP-16, and DFT-S OFDM with direct detection," *J. Lightw. Technol.*, vol. 35, no. 23, pp. 5127–5133, 2017.

- [4] N. Eiselt, et al., "Performance comparison of 112-Gb/s DMT, nyquist PAM4, and partial-response PAM4 for future 5G ethernet-based fronthaul architecture," J. Lightw. Technol., vol. 36, no. 10, pp. 1807–1814, 2018
- [5] N. Eiselt et al., "Evaluation of real-time 8 × 56.25Gb/s (400G) PAM-4 for inter-data center application over 80km of SSMF at 1550nm," J. Lightw. Technol., vol. 35, no. 4, pp. 955–962, 2016.
- [6] X. Zhou, R. Urata, and H. Liu, "Beyond 1 Tb/s intra-data center interconnect technology: IM-DD OR coherent?" J. Lightw. Technol., vol. 38, no. 2, pp. 475–484, 2020.
- [7] M. Xiang, Z. Xing, E. El-Fiky, M. Morsy-Osman, Q. Zhuge, and D. V. Plant, "Single-lane 145 Gbit/s IM/DD transmission with faster-than-Nyquist PAM4 signaling," *IEEE Photon. Technol. Lett.*, vol. 30, no. 13, pp. 1238–1241, Jul. 2018.
- [8] J. Zhou et al., "Joint FDE and MLSD algorithm for 56-Gbit/s Optical FTN-PAM4 System Using 10G-Class Optics," J. Lightw. Technol., vol. 37, no. 13, pp. 3343–3350, 2019.
- [9] M. Xu et al., "4×100G PAM-4 Transmission in Faster-than-Nyquist Systems Incorporating Eigenvalue-Space Precoding," in Proc. Opt. Fiber Commun. Conf., pp. M1J.7, 2018.
- [10] J. Zhang, J. Yu, N. Chi, and H.-C. Chien, "Time-domain digital preequalization for band-limited signals based on receiver-side adaptive equalizers," *Opt. Express.*, vol. 22, no. 17, pp. 20515–20529, 2014.
- [11] M. Guo et al., "112-Gb/s PAM4 with joint pre- and post-equalization for data center interconnects," in Proc. Asia Commun. Photon. Conf., 2019, Paper. T2G.2.
- [12] L. Zhang et al., "Beyond 100-Gb/s transmission over 80-km SMF using direct-detection SSB-DMT at C-band," J. Lightw. Technol., vol. 34, no. 2, pp. 723–729, 2015.
- [13] J. Zhang et al., "64-Gb/s/A downstream transmission for PAM-4 TDM-PON with Centralized DSP and 10G low-complexity receiver in c-band," in Proc. European Conf. Opt. Commun., 2017, pp. 1–3.
- [14] X. Tang, "Equalization scheme of C-band PAM4 signal for optical amplified 50-Gb/s PON," Opt. Express, vol. 26, no. 25, pp. 33418–33427, 2018.
- [15] X. Chen et al., "KramersCkronig receivers for 100-km datacenter interconnects," J. Lightw. Technol., vol. 36, no. 1, pp. 79–89, 2018.
- [16] C. Chen, X. Tang, and Z. Zhang, "Transmission of 56-Gb/s PAM-4 over 26-km single mode fiber using maximum likelihood sequence estimation," in *Proc. Opt. Fiber Commun. Conf.*, 2015, Paper Th4A.5.
- [17] S.-R. Moon, H.-S. Kang, H. Rha, and J. Lee, "C-band PAM-4 signal transmission using soft-output MLSE and LDPC code," *Opt. Express*, vol. 27, no. 1, pp. 110–120, 2019.
- [18] K. Zhang et al., "Intensity directed equalizer for the mitigation of DML chirp induced distortion in dispersion-unmanaged C-band PAM transmission," Opt. Express, vol. 25, no. 23, pp. 28123–28135, 2017.
- [19] Q. Hu et al., "50Gb/s PAM-4 Transmission Over 80-km SSMF Without Dispersion Compensation," in Proc. Eur. Conf. Opt. Commun., 2018, pp. 1, 2
- [20] X. Tang et al., "C-band 56-Gb/s PAM4 transmission over 80-km SSMF with electrical equalization at receiver," Opt. Express, vol. 27, no. 18, pp. 25708–25717, 2019.
- [21] C. Yang et al., "IM/DD based 112-Gb/s/lambda PAM-4 transmission using 18-Gbps DML," IEEE Photon. J., vol. 8, no. 3, pp. 1–7, Jun. 2016.
- [22] M. Xiang et al., "Experimental study of performance enhanced IM/DD transmissions based on constellation switching," Opt. Express, vol. 26, no. 12, pp. 15480–15489, 2018.
- [23] J. Jignesh et al., "Transmitter-side volterra filtering for increased dispersion tolerance in 56 gbaud PAM-4 systems," in Proc. Opt. Fiber Commun. Conf., 2018, Paper M2C.6.
- [24] X. Tang, Y. Qiao, and G. kung Chang, "Experimental demonstration of C-band 112-Gb/s PAM4 over 20-km SSMF with joint Preand Post-equalization," in *Proc. Opt. Fiber Commun. Conf.*, 2020, Paper W2A.46.
- [25] J. Zhou et al., "Transmission of 100-Gb/s DSB-DMT over 80-km SMF using 10-G class TTA and direct-detection," in Proc. Eur. Conf. Opt. Commun., 2016, pp. 1–3.
- [26] K. Zhong et al., "Digital signal processing for short-reach optical communications: A review of current technologies and future trends," J. Lightw. Technol., vol. 36, no. 2, pp. 377–400, 2018.
- [27] R. Rath, D. Clausen, S. Ohlendorf, S. Pachnicke, and W. Rosenkranz, "TomlinsonCHarashima precoding for dispersion uncompensated PAM-4 transmission with direct-detection," *J. Lightw. Technol.*, vol. 35, no. 18, pp. 3909–3917, 2017.